Assessing Cerebrovascular Reactivity by the Pattern of Response to Progressive Hypercapnia

Joseph A. Fisher,[1,2,3] Olivia Sobczyk,[2] Adrian Crawley,[4] Julien Poublanc,[4] Paul Dufort,[4] Lashmi Venkatraghavan,[3] Kevin Sam,[4] David Mikulis,[2,4] and James Duffin [1,3]*

[1]*Department of Physiology, University of Toronto, Toronto, Canada*
[2]*Institute of Medical Science, University of Toronto, Toronto, Canada*
[3]*Department of Anaesthesia and Pain Management, University Health Network, University of Toronto, Toronto, Canada*
[4]*Joint Department of Medical Imaging and the Functional Neuroimaging Laboratory, University Health Network, Toronto, Canada*

Abstract: Cerebral blood flow responds to a carbon dioxide challenge, and is often assessed as cerebrovascular reactivity, assuming a linear response over a limited stimulus range or a sigmoidal response over a wider range. However, these assumed response patterns may not necessarily apply to regions with pathophysiology. Deviations from sigmoidal responses are hypothesised to result from upstream flow limitations causing competition for blood flow between downstream regions, particularly with vasodilatory stimulation; flow is preferentially distributed to regions with more reactive vessels. Under these conditions, linear or sigmoidal fitting may not fairly describe the relationship between stimulus and flow. To assess the range of response patterns and their prevalence a survey of healthy control subjects and patients with cerebrovascular disease was conducted. We used a ramp carbon dioxide challenge from hypo- to hypercapnia as the stimulus, and magnetic resonance imaging to measure the flow responses. We categorized BOLD response patterns into four types based on the signs of their linear slopes in the hypo- and hypercapnic ranges, color coded and mapped them onto their respective anatomical scans. We suggest that these type maps complement maps of linear cerebrovascular reactivity by providing a better indication of the actual response patterns. *Hum Brain Mapp 38:3415–3427, 2017.*

Key words: cerebral blood flow; carbon dioxide; cerebrovascular reactivity

INTRODUCTION

Blood vessels in the brain react to the partial pressure of carbon dioxide in arterial blood ($PaCO_2$) by vasoconstricting in response to hypocapnia, and vasodilating in response to hypercapnia; consequently changing their resistance and altering blood flow. Since the ability to vasoconstrict and vasodilate is limited, the relation between a $PaCO_2$ stimulus, progressively rising from hypocapnia to hypercapnia, and a region's blood flow is sigmoidal [Battisti-Charbonney et al., 2011]. Moreover, when a high spatial and time resolved measure of regional blood flow is used, the patterns of the flow response in the whole brain as well as in large regions of interest (ROI) such as the grey matter (GM) and white matter (WM), also exhibit a sigmoidal shape [Bhogal et al., 2014, 2015; Sobczyk et al. 2014]. Nevertheless, it is common practice to approximate the sensitivity of the response as

*Correspondence to: James Duffin, Department of Physiology, University of Toronto, Toronto, Ontario, Canada, M5S 1A8. E-mail: j.duffin@utoronto.ca

Received for publication 24 May 2016; Revised 2 March 2017; Accepted 22 March 2017.
DOI: 10.1002/hbm.23598
Published online 3 April 2017 in Wiley Online Library (wileyonlinelibrary.com).

the slope of a linear regression between $PaCO_2$ and flow, currently referred to as the cerebrovascular reactivity (CVR). We note that CVR refers to the change in *flow*—rather than resistance—in response to $PaCO_2$.

Three assumptions underlie CVR as a measure reflecting vascular response. First, a suitable high spatial and time resolved measure of regional blood flow is available. Second, fitting a single line to a sigmoidal curve will provide a reasonable approximation of the sensitivity of the vascular response to $PaCO_2$ [Pillai and Mikulis, 2015]. And third, localized changes in flow represent local changes in resistance.

This latter assumption can be challenged; we [Sobczyk et al., 2014] and others [Bhogal et al., 2015] hypothesise that flow responses are a mixed result of resistance changes and competition for flow between regions. The explanation for the conditions for competition for flow follows from the anatomical and physiological configuration of the cerebral vasculature. When upstream blood flow is not limiting, blood flow is supplied to regions perfused in parallel, according to their individual resistances. However, when downstream flow demand exceeds supply, flow to each region depends on its relative resistance, as the parallel perfused regions compete for flow [Sobczyk et al., 2014]. Such competition for flow in the brain is a consequence of the major arteries supplying the brain having the largest resistance to flow of any organ [Faraci and Heistad, 1990]. This arrangement applies at every level, from the capillary level to that of the carotid arteries resulting in a fractal pattern of blood distribution.

In healthy people, the changes in resistance with $PaCO_2$ are finely balanced between vascular regions throughout the brain so most regions exhibit a sigmoidal pattern of flow response [Bhogal et al., 2015], and a linear regression measurement provides a reasonable estimate of CVR. However, in the presence of cerebrovascular pathophysiology, the finely balanced changes in resistance are disrupted and net regional flow response patterns to a linear increase in stimulus may be more complex.

In this regard, when interrogating Blood Oxygen Level Dependent (BOLD) changes in patients with steno-occlusive disease subjected to a progressively increasing CO_2 stimulus, we had observed in many voxels a variety of response patterns to which a sigmoidal curve could not be readily fit. In particular some voxels manifested reductions in BOLD signal, biphasic responses, some with initial increases in BOLD signal followed by reductions in signal as PCO_2 increased further [see Fig. 6 in Sobczyk et al., 2014], and some the reverse.

We considered that restricting CVR calculations by forcing the fitting of the data to a straight line would obscure the biphasic patterns of BOLD response. Consequently, as a high level screen for the frequency and distribution of the various shaped BOLD signal responses to progressive hypercapnia, we classified them into four general patterns by the signs of their slopes at $P_{ET}CO_2$ levels above and below the resting $P_{ET}CO_2$ (i.e., +/+, +/−, −/−, −/+). Choosing to split the response at resting $P_{ET}CO_2$ was based on the notion that the hypercapnic range tests the vasodilatory responsiveness, whereas the hypocapnic range tests the vasoconstictive responsiveness. The two line slope sign description of these responses we adopted is simply a first step in assessing the prevalence of different response patterns.

We reasoned that in all voxels with sigmoidal curves, both halves of the graph would have a positive slope. In the course of identifying the locations of voxels with sigmoidal responses we also found large ROI with each of four combinations of slopes; non sigmoidal slopes were particularly prevalent in patients with steno-occlusive cerebral vascular disease.

The objective of this article therefore became the classification of the four different patterns of response observed as type A, a positive linear pattern, rising in hypo- and hypercapnia; type B, an inverted U-shaped pattern, rising in hypocapnia and falling in hypercapnia; type C, a negative linear pattern, falling in hypo- and hypercapnia, and type D, a U-shaped pattern, falling in hypocapnia and rising in hypercapnia.

We investigated the frequency and distribution of the various response patterns in a sample of healthy subjects and patients with steno-occlusive cerebral vascular disease. Finding that the different patterns were not dispersed, but tended to cluster in large contiguous regions of the brain, suggested that shared physiology underlies specific patterns, and that pursuit of this physiology would likely add value to CVR assessment.

METHODS

Subjects

We made voxel-wise surveys of the patterns of BOLD response to a progressive, hypo- to hypercapnic, CO_2 stimulus in 18 (7F) healthy subjects, mean (SD) age 36.2 (13.8), and 10 (4F) patients, mean (SD) age 46.7 (13.1), with clinical symptoms and/or known cerebrovascular disease. The control subjects claimed to be in good health, denied a history of neurological disease, were non-smokers, and were taking no medications. The patients were selected from our database and originally were recruited for CVR studies because they had recent neurologic symptoms thought to be vascular in origin or were known to have chronic cerebrovascular disease. The control subjects were selected from a study that developed a reference atlas of normal CVR [Sobczyk et al., 2015]. Both studies conformed to the standards set by the latest revision of the Declaration of Helsinki, and were approved by the Research Ethics Board of the University Health Network and Health Canada. All subjects were competent and gave written informed consent. Subjects were asked not to engage in heavy exercise or drink caffeinated drinks on the day of the test.

Experimental Protocol

CO_2 stimulus

Subjects were fitted with a facemask and connected to a sequential gas delivery breathing circuit [Somogyi et al.,

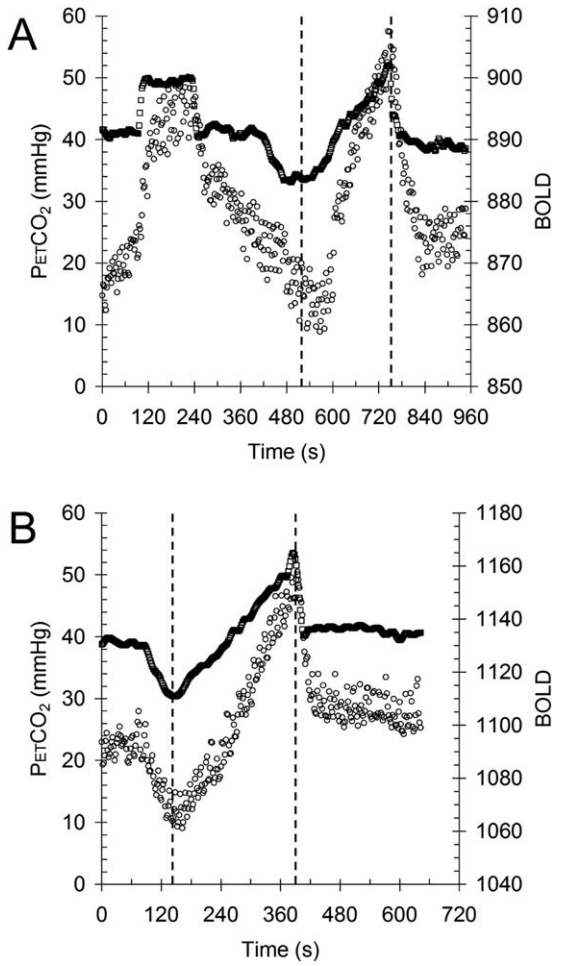

Figure 1.

The stimulus paradigms. A) Patients. B) Controls. Square symbols = end tidal PCO_2 ($P_{ET}CO_2$) and circle symbols = mean GM BOLD response versus time. Analysis was confined to the ramp portion of the data between the dashed lines.

2005]. The patterns of end-tidal (i.e., at the end of exhalation) partial pressure of CO_2 ($P_{ET}CO_2$) and oxygen ($P_{ET}O_2$) were programmed into an automated gas blender (RespirAct™, Thornhill Research Inc., Toronto, Canada) running the prospective gas targeting algorithm of Slessarev et al. [2007]. The implementation of prospective end-tidal gas control is described in greater detail elsewhere [Fierstra et al., 2013; Slessarev et al., 2007].

The sequence for patients consisted of clamping $P_{ET}CO_2$ at the subject's resting baseline for 1 min, a step increase by 10 mm Hg for 2 min followed by 2 min at baseline. Then $P_{ET}CO_2$ was slowly reduced by 10 mm Hg over 30 sec, followed by a steady rise in $P_{ET}CO_2$ to 15 mm Hg above baseline over 4.3 min, and a return to baseline for 2 min (Fig. 1). The gas sequence for control subjects was simpler; after 2 min at resting $P_{ET}CO_2$, $P_{ET}CO_2$ was slowly reduced by 10 mm Hg over the next 3 min. Then, $P_{ET}CO_2$ was slowly increased to 15 mm Hg above resting, and returned to resting for 3 min.

MRI protocol

Magnetic resonance imaging was performed with a 3.0-Tesla scanner (Signa HDx; GE Healthcare, Milwaukee, Wisconsin) with an 8-channel phased-array head coil and consisted of BOLD acquisitions using gradient echo planar imaging (EPI) gradient echo. Sequence parameters were slightly different between the healthy and patient groups (TR/TE = 2,000/30 ms, field of view 24 × 24 cm, matrix size 64 × 64, number of frames = 333, slice thickness 3.5 mm, and flip angle = 70° for the patient group and TR/TE = 2,000/30 ms, field of view 24 × 24 cm, matrix size 64 × 64, number of frames = 405, slice thickness 3 mm, and flip angle = 80° for the healthy group). The acquired MRI and $P_{ET}CO_2$ data were analysed using AFNI software [Cox, 1996]. BOLD images were then volume registered and slice-time corrected and co-registered to an axial 3-D T1-weighted Inversion-Recovery prepared Fast Spoiled Gradient-Echo (IR-FSPGR) volume (TI/TR/TE = 450/8/3 ms, matrix size 256 × 256, field of view 22 × 22 cm, slice thickness = 1 mm, and flip angle = 15°) that was acquired at the same time [Saad et al., 2009]. $P_{ET}CO_2$ data was re-sampled at TR, and time-shifted to the point of coincidence between the rapid decrease in $P_{ET}CO_2$ at the end of the ramp and that of the whole brain average BOLD signal. The time shift is done to time align the BOLD and $P_{ET}CO_2$ data that were recorded on different computers. The amount of shift therefore has no physiological significance as the data acquisitions were not synchronized.

CVR and type calculations. CVR was calculated from the slope of a linear, least-squares fit of the BOLD signal data series to the $P_{ET}CO_2$ data series over the range of $P_{ET}CO_2$ represented by the ramp portion of the CO_2 sequence on a voxel-by-voxel basis. The slopes were color-coded to a spectrum of colours corresponding to the direction (positive or negative) and the magnitude of the correlation and overlaid over the corresponding structural scans to form CVR maps. This method has been described in greater detail by Sobczyk et al. [2014].

To classify the pattern of response over the range of $P_{ET}CO_2$ represented by the ramp portion of the CO_2 sequence, the BOLD signal was divided into hypocapnic and hypercapnic ranges based on the resting $P_{ET}CO_2$. A linear least squares fit of each range yielded two slopes, which were used to categorise the response patterns into types by the combination of signs of the slopes of straight lines fitted to the first and second halves of the BOLD response as follows: A +/+, B +/−, C −/− and D −/+. If either slope were within the range of ±0.01 it was considered to be zero and no classification was applied. Figure 2 illustrates these procedures.

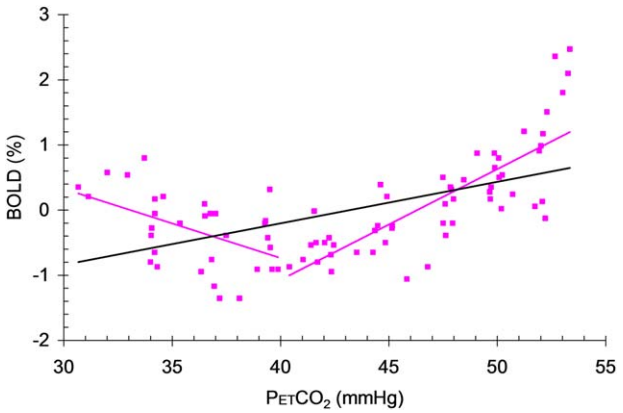

Figure 2.
An example illustrating the CVR and pattern type calculations. Purple filled square symbols = a single voxel BOLD response to $P_{ET}CO_2$ fitted with a single black line (slope = CVR), and two purple lines whose slope signs were used to categorise the response pattern type (here, D = −/+).

Statistical calculations

Comparisons of type prevalence between grey matter (GM) and white matter (WM) and between patients and controls were made using two-way analysis of variance (SigmaPlot 12.5) with factors patients versus controls and GM versus WM and all pairwise multiple comparison procedures (Holm–Sidak method). Similarly, separate comparisons of type prevalence for GM and WM in controls and in patients were made using two-way analysis of variance (SigmaPlot 12.5) with factors type (A +/+ vs. B +/− vs. C −/− vs. D −/+) and GM versus WM. Linear fits were assessed as r^2.

RESULTS

Response Pattern Types

Figure 3 shows examples of individual voxel plots of BOLD signal versus $P_{ET}CO_2$ illustrating the four distinct patterns of BOLD response to CO_2: A +/+, B +/−, C −/− and D −/+.

Type Maps

Each of the four types of BOLD response patterns shown in Figure 2 were colour coded (A +/+ = red, B +/− = light blue, C −/− = dark blue, and D −/+ = yellow) and the colours were superimposed on the corresponding voxel of the anatomical scan to produce type maps. Figure 4 shows a comparison of CVR and type maps for a healthy individual, illustrating the additional detailed information provided by the type map. The CVR map shows that CVR is higher in the GM than the WM. The type map shows, in addition, that the response in the WM is not lower than that of GM but of type D −/+. Because of the biphasic pattern of response, fitting a straight line to the data will necessarily result in a shallow slope; in this case, the predominant slope is positive (i.e., positive CVR). The type map also shows areas of type B +/− where the BOLD response increases with initial increases in PCO_2 but decreases at the higher PCO_2 as type A +/+ voxels steal their flow. As with the D −/+ type, the CVR for type B +/− in this example will be small, and most voxels exhibit a positive slope when a single line is fitted to the BOLD data.

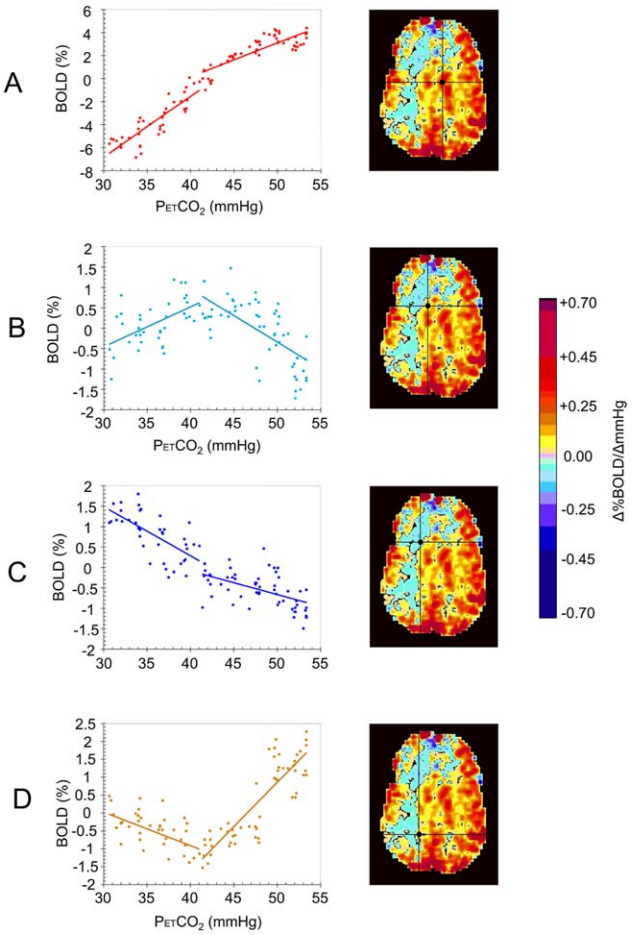

Figure 3.
Example plots of BOLD MRI responses to a global ramp increase in $P_{ET}CO_2$ from 30 to 55 mm Hg for an 18-year-old male patient (p2) with a history of Moyamoya disease affecting the right MCA territory. The voxel locations are indicated by the cursors on the CVR maps. **A**) A positive response with a sigmoidal shape. **B**) An initial positive response which then declines. **C**) A response which simply declines. **D**) A response that initially declines but then increases. These four types of response pattern were used to classify the response patterns of the voxels in healthy subjects and patients.

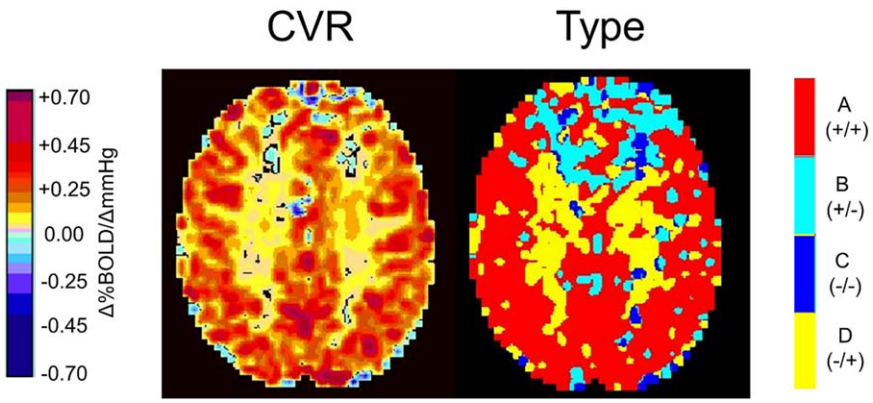

Figure 4.

Example CVR and type maps for an axial slice obtained from analysis of BOLD MRI responses to a ramp CO_2 stimulus in a healthy 75-year-old male (c2). The colour scales are as shown. The WM in this subject shows a positive CVR whereas the type map indicates that the pattern of flow in the WM is biphasic (D −/+ type). In the frontal lobes, the flow is also biphasic (B +/− type). The biphasic aspect of both B +/− and D −/+ patterns results in small CVR values.

Control Type Maps

Figure 5 shows a comparison of CVR and type maps for the cohort of 10 healthy subjects, and Table I lists the prevalence of the types for each subject.

In healthy subjects, CVR maps show little apparent differences between subjects whereas type maps show marked differences between subjects. GM voxels in the type maps are mostly A +/+ type as expected, with some subjects showing B +/− and D −/+ types, and no C −/− type; frontal areas were frequently B +/− type. WM is also mostly A +/+ type, but some subjects may have some B +/−, C −/− and D −/+ types, accounting for the WM steal seen in the CVR [see Mandell et al., 2008a]. We observed only small spots of C −/− type.

Patient Type Maps

Figure 6 provides a detailed comparison of CVR and type maps for two patients. Visual inspection shows that the first patient (p1) has poor CVR in the GM and WM of both frontal and temporal lobes. The type map classifies these as having the biphasic D −/+ type of flow response pattern. Such a widespread area of D −/+ pattern including grey matter was not seen in any of the healthy subjects. The second patient (p2) shows extensive areas of B +/− and D −/+ type patterns. The type map identifies which negative CVR regions are due to steal (C −/− type) rather than a response that fails at high CO_2 (B +/− type). The direction of the two slopes in the biphasic B +/− and D −/+ patterns are opposite so they tend to counteract each other, with CVR interpreted as positive or negative depending on which slope predominates in number and position of points. Consistently, over all patient scans, the A +/+ type pattern was always interpreted as positive CVR and the C −/− type pattern always indicated negative CVR. In Figure 6, the areas of C −/− type for patient p2 are outlined by a purple line and mapped onto the CVR map. It shows that the C −/− type resides within the core of the negative region of the CVR map. We elaborate on these observation in the discussion.

Figure 7 shows a comparison of CVR and type maps for the remaining eight patients of the patient cohort. Table II lists patient descriptions, and Table III lists the prevalence of the types for all patients.

In contrast to the healthy cohort, patient type maps all showed extensive areas of B +/−, C −/− and D −/+ types in both WM and GM. The C −/− type was always associated with negative CVR (areas of steal). Both negative and positive CVR were seen in B +/−, and D −/+ types as a result of the vagaries of fitting a straight line to biphasic curves. Similarly, the biphasic nature of B +/− and D −/+ types resulted in small CVR values when fitted by a straight line.

Table IV shows the results of a 2-way analysis of variance with all pairwise multiple comparison procedures (Holm–Sidak method) with factors GM versus WM and patients versus controls. Only the prevalence of type B +/− did not differ between GM and WM, and only the prevalence of type D −/+ did not differ between patients and controls. Comparing male and female type prevalence in the control group showed no significant differences for GM or WM. A regression of the type prevalence's with age in the control group showed no significant trends for either GM or WM.

A comparison of the prevalence of the different types in GM and WM using a 2-way analysis of variance with all pairwise multiple comparison procedures (Holm–Sidak method) with factors GM versus WM and types showed the following: In the control group the prevalence of types in GM and WM all differed except for types D −/+ and B

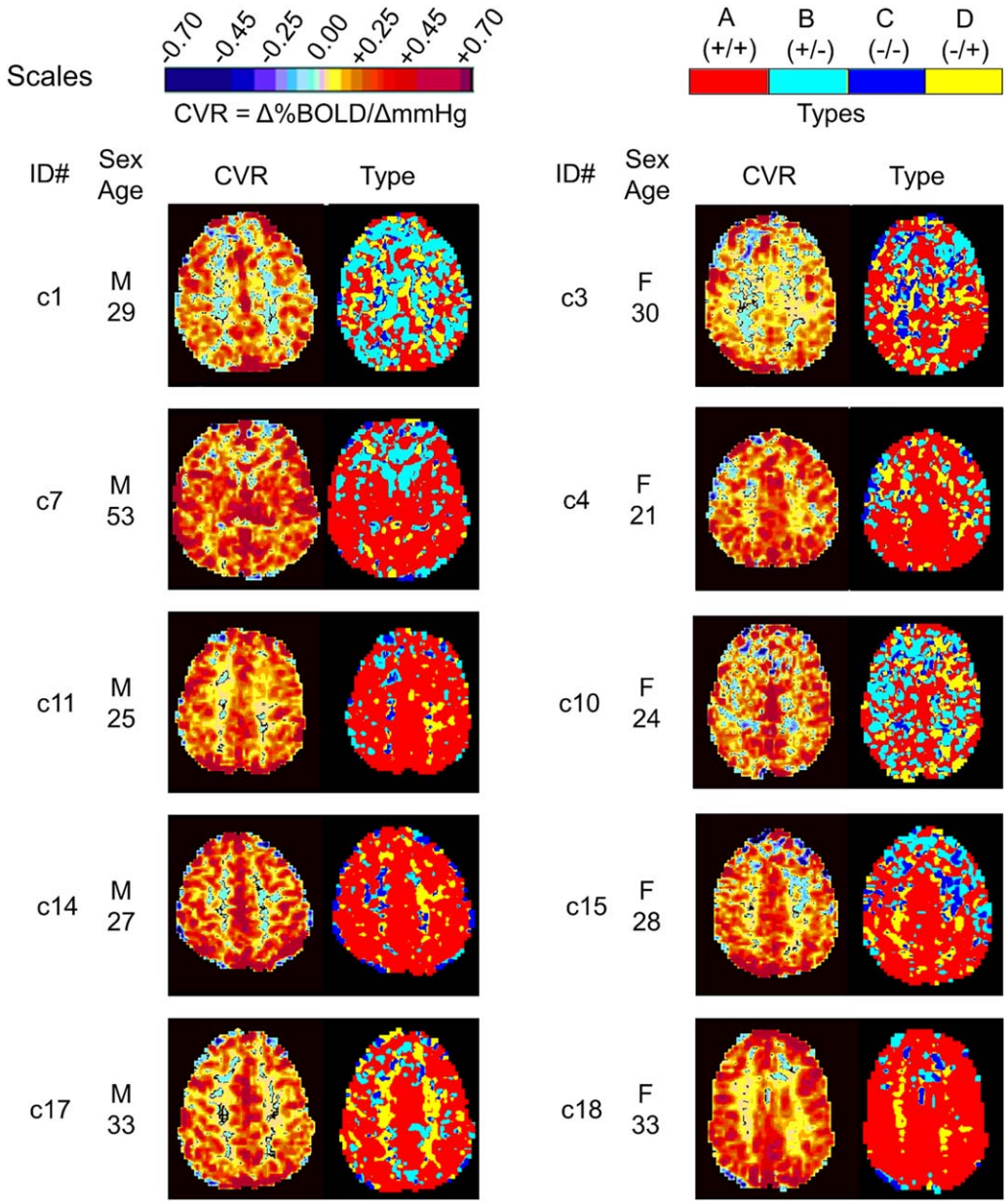

Figure 5.
A comparison of CVR and type maps for the healthy cohort demonstrating the range of expected type patterns.

+/−, which did not differ in WM. In the patient group the prevalence of types D −/+ and C −/− did not differ in the GM, whereas in the WM the only differences were between types A +/+ and C −/− and types A +/+ and D −/+.

DISCUSSION

Our examination of the voxel by voxel patterns of the BOLD MRI response to a ramp CO_2 challenge from hypo- to hypercapnia in both healthy control subjects and patients confirmed our prediction of widespread prevalence of voxels with complex response patterns. For many voxels, in both healthy control subjects and patients with cerebrovascular pathophysiology, response patterns were not well described by a sigmoidal response pattern. Therefore, application of a linear fit to the response is inappropriate for calculating CVR. The simple metric we introduced for the observed response patterns, dividing the response to CO_2 into hypo- and hypercapnic ranges,

TABLE I. The prevalence (%) of the types and mean (SD) CVR in the whole brain for the 18 healthy subjects

ID #	Sex	Age yrs	%A		%B		%C		%D		GM CVR Mean (SD)	WM CVR Mean (SD)
			GM	WM	GM	WM	GM	WM	GM	WM		
C1	m	29	49.3	28.7	31.7	35.2	2	8.5	17.1	27.5	0.30 (0.43)	0.10 (0.21)
C2	m	75	77.8	52.9	10	16.7	1.5	24.2	10.7	24.2	0.25 (0.35)	0.09 (0.13)
C3	f	30	65.7	46.7	19.5	17.9	6.3	14.9	8.5	20.5	0.24 (0.42)	0.08 (0.19)
C4	f	21	66.6	62	18.6	18.1	4.5	5.7	10.4	14.2	0.33 (0.52)	0.20 (0.26)
C5	m	53	59.7	40.1	25.3	26.6	4.5	12.6	10.5	20.7	0.25 (0.34)	0.09 (0.2)
C6	f	26	66.2	50.3	20.2	20.2	4.2	9.3	9.3	20.3	0.26 (0.39)	0.12 (0.2)
C7	m	53	73	61.1	16.5	16.7	3.2	5.6	7.3	16.6	0.43 (0.85)	0.17 (0.39)
C8	m	27	68.7	39.9	18.2	18.6	5.7	18.8	7.4	22.7	0.44 (0.75)	0.11 (0.31)
C9	f	47	67.6	52.5	18.3	22.2	4.6	8.7	9.5	16.6	0.26 (0.41)	0.12 (0.2)
C10	f	24	48.3	36	29.8	28	5.5	8.7	16.4	27.2	0.24 (0.42)	0.11 (0.22)
C11	m	25	82.7	70.6	7.6	10.5	4.3	6.9	5.5	12	0.30 (0.4)	0.12 (0.17)
C12	m	44	75	55.6	17.3	22.7	2.5	7.7	5.2	14	0.30 (0.34)	0.11 (0.15)
C13	m	36	89.1	76.4	6.9	12.9	1.8	4.1	2.2	6.5	0.32 (0.38)	0.14 (0.15)
C14	m	27	78.9	63.9	11.8	12.5	3.2	5.9	6.1	17.7	0.33 (0.4)	0.13 (0.19)
C15	f	28	84.9	66.3	3.6	7	3.2	8.4	8.3	18.3	0.41 (0.58)	0.17 (0.32)
C16	m	41	68.4	50.3	12.9	13.6	7	14.2	11.7	21.9	0.33 (0.45)	0.12 (0.23)
C17	m	33	68.1	54.9	13.3	17.8	3.4	5.6	15.2	21.8	0.42 (0.63)	0.20 (0.29)
C18	f	33	80.8	65.3	10.5	10.1	2	3.2	6.7	21.5	0.33 (0.39)	0.15 (0.25)

recognizes the presence of biphasic responses and thus provides a more nuanced classification into four types based on the signs of the linear slopes in each range below and above resting PCO_2. These types and their associated anatomical maps provide a more detailed description of the distribution of cerebrovascular response to CO_2.

To confirm the assumption that the 2-slope model has to be a better fit to the responses than the 1-slope model we compared their r^2 values for each subject. As expected, the r^2 values for the 2-slope model are indeed significantly greater than those of the 1-slope model (t-test, $P < 0.001$). The ensemble average mean (SD) r^2 for the 1-slope versus

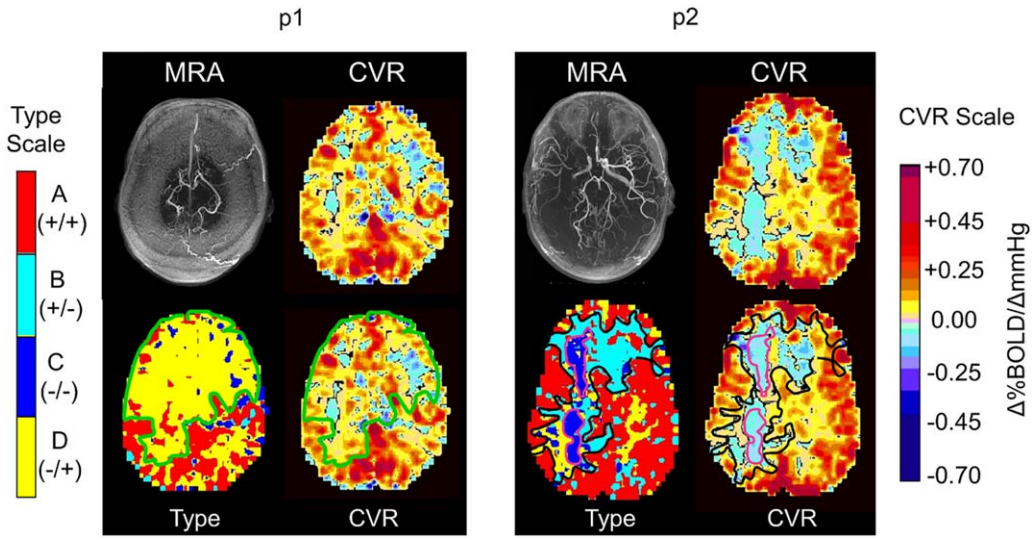

Figure 6.

Example detailed comparisons of CVR and types maps for two patients. A detailed examination of these maps is given in the discussion. For p1, the type map (bottom row left), the voxels with D −/+ are outlined (green line) and reflected onto the CVR map (green line, bottom row, right). For p2, the type map (bottom row, left) the voxels with B +/− are outlined in black, and the C −/− in purple. These are reflected onto the CVR map (bottom row, right). Note that the biphasic D −/+ are interpreted as positive and negative CVR. In p2, the biphasic B +/− are interpreted as positive and negative CVR, but the monophasic C −/− are only negative CVR, or steal.

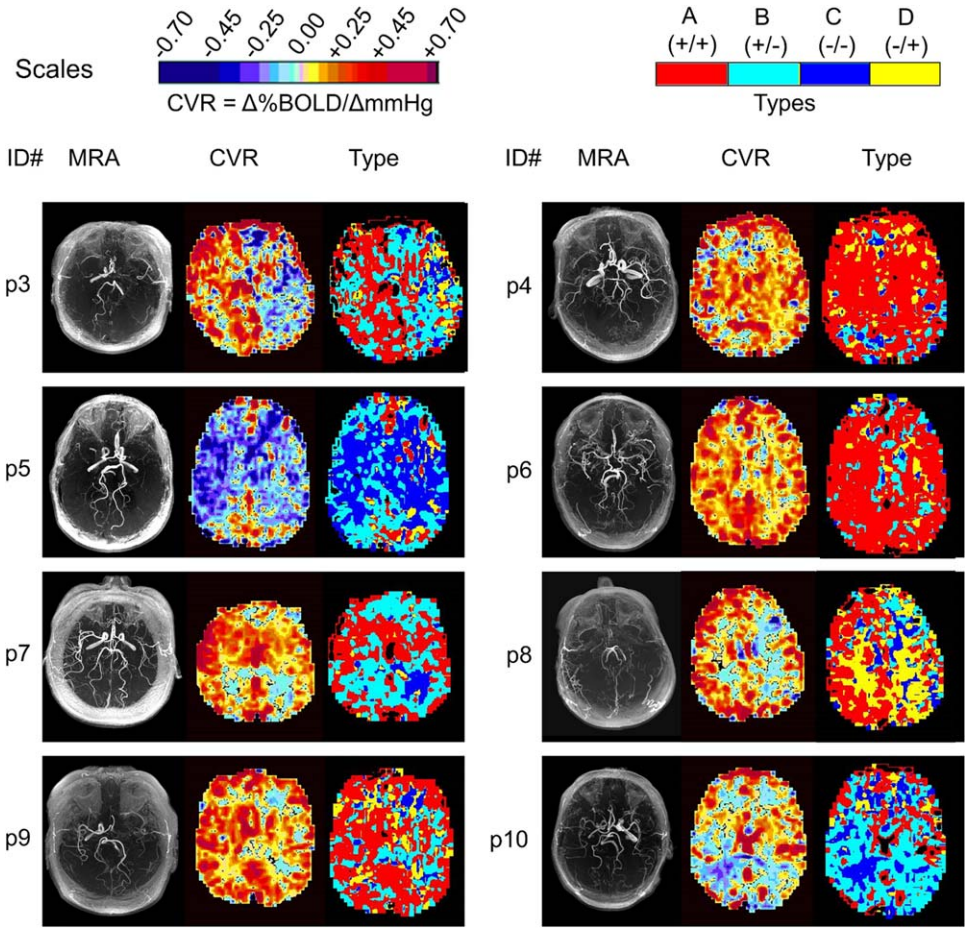

Figure 7.
A comparison of CVR and type maps for patients. A detailed examination of these maps is provided in Table V in the discussion.

TABLE II. Patient descriptions

Patient ID	Sex	Age	Condition
p1	M	53	Moyamoya disease, RSTA to pial synangiosis, ICH and IVH, currently asymptomatic
p2	M	18	History of Moyamoya disease affecting the right MCA territory.
p3	M	58	LICA stenosis, L parietal stroke with R hemiparesis, moderate to severe cognitive impairment
p4	M	60	Distal PCA aneurysm, R MCA stenosis, 2 periventricular grey matter heterotopia, IVH
p5	M	47	Bilateral moyamoya, L stroke, headaches
p6	F	49	Recurring TIAs, R sided stroke, coronary artery disease, quadruple CABG, aortic atherosclerosis
p7	F	51	Moyamoya, stroke, TIAs, LSTA-MCA bypass
p8	F	32	Iatrogenic moyamoya disease, R EC-IC bypass, diagnosed with optic glioma had radiation and surgery, VP shunt
p9	M	57	L ICA occlusion, cognitive decline, L hemispheric hypoperfusion, R hemiparesis episodes
p10	F	42	Bilateral ICA stenosis, calcifications, reoccurring headaches with upper body paresthesias

Abbreviations: L, left; R, right; ICA, internal carotid artery; PCA, posterior cerebral artery; ICH, intracerebral haemorrhage; IVH, interventricular haemorrhage; TIA, transient ischemic attack; LSTA, left superficial temporal artery; RSTA, right superficial temporal artery; MCA, middle cerebral artery; EC, external carotid; IC, internal carotid.

TABLE III. The prevalence (%) of the types in the whole brain for the 10 patients

ID	Sex	Age yrs	%A		%B		%C		%D		GM CVR Mean (SD)	WM CVR Mean (SD)
			GM	WM	GM	WM	GM	WM	GM	WM		
p1	M	53	49.1	35.4	6.2	4.8	10.9	13.7	33.8	46.1	0.22 (0.29)	0.10 (0.17)
p2	M	18	59.6	40.5	27.9	27.7	2.5	9.3	10	22.5	0.26 (0.42)	0.09 (0.18)
p3	M	58	45.7	39.4	36.9	39.9	5.5	9	11.9	11.7	0.21 (0.46)	0.08 (0.33)
p4	M	60	72.2	51.8	12.3	12.1	6.2	14.9	9.2	21.2	0.25 (0.45)	0.09 (0.22)
p5	M	47	22.1	15.3	44.9	36.4	24	38.2	9	10.1	0.0 (0.89)	−0.05 (0.36)
p6	F	49	74.9	61.3	16.8	17.7	4.4	9.1	3.8	11.8	0.29 (0.38)	0.12 (0.22)
p7	F	51	46.1	30.3	43.9	40.4	3.2	13.4	6.8	15.9	0.21 (0.34)	0.08 (0.19)
p8	F	32	53.2	46.8	11.3	11.6	10.5	11.8	25	29.8	0.28 (0.63)	0.24 (0.65)
p9	M	57	63.6	42.2	23.7	27.7	2.4	9.6	10.3	20.5	0.33 (0.46)	0.14 (0.29)
p10	F	42	26.8	10.3	51.5	41.9	16.9	42.4	4.7	5.4	0.08 (0.45)	−0.05 (0.23)

2-slope model in control subjects was 0.47 (0.3) versus 0.55 (0.27), and in patients was 0.25 (0.23) versus 0.31 (0.22).

Three of the four pattern types we categorised (A +/+, B +/−, C −/−) have been reported previously [Sobczyk et al., 2014] in a study that discussed steal (Type C) and the differences between CVR at different ranges of CO_2 stimulus. In this study we surveyed CVR responses for the different types so as to create type maps, and found another biphasic type (D −/+) where the BOLD response slope decreases as CO_2 increases from hypocapnia to normocapnia and then increases as CO_2 increases from normocapnia to hypercapnia. Because the previous study concentrated on modelling steal and not classifying the responses according to type as described in this article we missed noticing the type D −/+ responses, although they are abundantly present in retrospect. We suggest that the patient type maps provide an alternative and enhanced view of cerebrovascular reactivity. Table V provides our theoretical interpretation of the patient type maps, and in the following paragraphs we discuss the two patients shown in Figure 6.

Patient p1 was a 53-year-old male with symptomatic Moyamoya disease and a previous revascularization attempt by transposing a flap containing the right superficial temporal artery to the surface of the brain, (encephalo-duro-arteriosynangiosis; EDAS), who is currently asymptomatic. The angiogram (MRA) shows complete occlusion of both internal carotid arteries, and the CVR (top right) shows an absence of a robust CVR in the GM, which does not lateralize. The type map shows extensive areas of D −/+ type pattern bilaterally, particularly on the right. An outline of the D −/+ type area projected onto the CVR map (lower right) shows the reason for the low CVR in GM biphasic aspect of the response pattern. The type map also shows that the A +/+ type regions are the only normally responding CVR voxels. This information was not apparent from the CVR map alone.

Patient p2 was an 18-year-old male with a history of Moyamoya disease affecting the right MCA territory. The angiogram (MRA) shows an occlusion of the right distal internal carotid artery (left in the figure). The CVR (top right) shows steal predominantly in the right WM. The type map shows predominantly B +/−, C −/− and D −/+ types on the right side (left in the figure) in a more extensive area of the white matter than the negative area (blue) in the CVR map, as seen on an outline of B +/−, C −/− and D −/+ types reflected on to the CVR map (lower right). It indicates that the B +/− type can have positive (yellow-red) or negative (blue) CVR slopes. However C −/− type (seen in the purple outline and coloured dark blue in the type map) indicates negative CVR and steal over the entire CO_2 range. This type map therefore illustrates the ability to separate positive slope CVR responses into two forms, normal (response always positive to increasing CO_2) and abnormal (initially positive but then negative responses to increasing CO_2), as well as areas of complete steal (type C −/−).

At least in these patients, type scoring enhances the interpretation of the conventional CVR map. For regions of positive CVR, the A +/+ type denotes a healthy response and the CVR metric reflects this strength accurately. For areas with biphasic responses that have a

TABLE IV. Comparison of patients versus controls for the prevalence of types; mean (SEM)

	%A		%B		%C		%D		CVR	
	GM	WM	GM	WM	GM	WM	GM	WM	GM	WM
patients	51.3 (5.5)	37.3 (4.9)	27.6 (5.1)	26.0 (4.3)	8.70 (2.2)	17.2 (3.9)	12.4 (3.0)	19.5 (3.7)	0.21 (0.03)	0.08 (0.03)
controls	70.6 (2.6)	54.1 (3.0)	16.2 (1.8)	18.2 (1.6)	3.9 (0.4)	9.6 (1.3)	9.3 (0.9)	19.1 (1.2)	0.32 (0.02)	0.13 (0.01)
GM vs. WM	**$P < 0.001$**		$P = 0.953$		**$P < 0.001$**		**$P < 0.001$**		**$P < 0.001$**	
patients vs. controls	**$P < 0.001$**		**$P < 0.001$**		**$P < 0.001$**		$P = 0.166$		**$P < 0.001$**	

TABLE V. Suggested interpretations for the Patient Type maps shown in Figure 7

Patient	CVR	Types map
p3	RH positive CVR (normal appearing). LH mostly negative (steal).	RH much of the positive CVR is type B +/−. An example of positive CVR but biphasic pattern which is not seen in normal cohort. LH steal types B +/− and D −/+. Most severe steal on CVR confirmed as type D −/+.
p4	RH has reduced CVR particularly in right occipital lobe; LH appears normal.	RH negative areas of CVR are indeed biphasic type D −/+. One area in occipital lobe is complete steal (type C −/−). LH predominantly type A +/+, consistent with the normal type and extent of the CVR response
p5	Extensive bilateral steal	Negative CVR is types B +/− and C −/−. Vessels in type B +/− have been shown to have increased flow for small increases in PCO_2 and may be stealing from the type C −/− which reduce their flow from initial increases in PCO_2.
p6	Normal appearing CVR other than over the ventricles.	Extensive type A +/+ with types B +/− and C −/− over the ventricles. CVR is normal in degree and type. Presumably this patient has a well developed collateral circulation.
p7	Areas of negative CVR (steal) in occipital lobe WM bilaterally. (Frontal lobes often contain susceptibility artefacts and are not usually diagnostic).	Confirmation of negative CVR as type B +/−. Type C −/− identifies the complete steal.
p8	RH good CVR in cortical areas, negative CVR (steal) in WM. Extensive negative CVR (steal) in LH WM and a small region of left parietal GM.	RH cortical areas type A +/+ consistent with CVR. WM type D −/+ bilaterally. LH positive cortical CVR is type B +/− showing low CVR in areas of positive CVR.
p9	Normal CVR right hemisphere. Negative CVR (steal) in LH WM.	RH: Type A +/+ confirms normal CVR. LH cortex is type B +/− indicating abnormal positive CVR. Type C −/− also identifies area of complete steal. There are type C −/− and D −/+ responses in LH WM.
p10	Negative CVR (steal) in WM bilaterally, and in the inferior division right MCA (posterior temporal) and left PCA. (occipital) GM.	Much of the positive CVR is actually type B +/−. Areas of complete steal (type C −/−) nicely demonstrated in right MCA left PCA GM and WM.

Abbreviations: RH, right hemisphere; LH, left hemisphere; CVR, cerebrovascular reactivity; WM, white matter; GM, grey matter. MCA, middle cerebral artery.

positive component (B +/− and D −/+ types), CVR indicates the preponderance of the change in flow (positive or negative) and its slope may in some degree relate to the overall severity of vascular dysfunction, but the true response is indicated more accurately by the distribution of B +/− and D −/+ types. For areas with biphasic responses that have a negative component (B +/−, C −/−, and D −/+ types), CVR may be predominantly negative but could have a positive slope in some instances. Only separation of the response into B +/−, C −/−, or D −/+ types will separate complete steal over the entire $P_{ET}CO_2$ range [type C −/− as described by Mandell et al., 2008b; Poublanc et al., 2013; Sobczyk et al., 2014] from the other biphasic possibilities (B +/− and D −/+ types) where steal only occurs over a small range of $P_{ET}CO_2$. It has been suggested that B +/− type patterns arise when the flow in vascular beds with reduced vasodilatory reserve compete with beds with greater reserves [Sobczyk et al., 2014]. As the D −/+ type occurs in contiguous voxels over large regions of interest they too are very likely to have a consistent underlying pathophysiology, but this type has not previously been reported and the pathophysiology unknown. We are just beginning to examine the distribution of the four major types in patients and it is becoming apparent that there are major differences in the prevalence and distribution in the types between healthy subjects and patients. The clinical relevance of these differences remains to be determined.

Explanation for the Response Types

In searching for a possible origin of these response patterns we start with the cerebrovascular anatomy. A CO_2 stimulus has a direct effect on the cerebrovascular resistance to blood flow, with a linear range of increasing $PaCO_2$ resulting in a sigmoidal reduction in resistance. However, monitoring the BOLD signal or any other flow-related measure, does not assess resistance, but rather flow. In a linear conduit, pressure, resistance and flow are linked so assessing flow provides information about resistance. But the blood flow to the brain is not organized according to a linear response system. There are four main extracranial vessels with circle of Willis and pial anastomoses within the skull, as well as potential anastomoses between intracranial and extra-cranial vessels through

transosseous anastomoses. Thus, in contrast to a linear system, the changes in flow in any cerebral vascular bed or region also reflect the pattern of changes in resistance of the vessel beds with which it is being perfused in parallel. We theorise that the patterns of flow response we observed reflect this phenomenon. For example, in health, the changes in resistance are presumably balanced such that the flow to each voxel reflects its change in resistance, resulting in a predominance of the type A +/+ response pattern. In the presence of cerebrovascular disease, we theorise there exists upstream limitation in blood flow forcing downstream regions perfused in parallel to compete for flow. Under these conditions, the balance in flow operating in health is disrupted precipitating one of the other three distinct flow patterns (B +/−, C −/−, D −/+) we describe. To be clear: our hypothesis is that if we were able to measure resistance, we expect that resistance would still fall with progressive hypercapnia in a sigmoidal manner in each vessel; but interactions with the sigmoidal changes in resistance of the other beds in the vascular unit could produce flow response patterns of the various types observed.

We suggest that this competition model can occur on different scales. For example, in patients with unilateral haemodynamically significant stenosis, the ipsilateral hemisphere undergoes steal and the contralateral hemisphere is the 'thief'. We have published many such examples, for example, Poublanc et al. [2015]. However, one can conceive that this may occur at progressively smaller scales, down to between capillaries perfused by a common feeder vessel. And it may occur at size scales everywhere in-between. Thus, in a vascular system with multiple vasculopathies, the steal and the thief vessels constitute a fractal and a redundant pattern such that a vessel steals from a collateral bed, but is being stolen from by another vessel which has more vasodilatory reserve but ultimately not enough to prevent it from perhaps undergoing steal itself.

Limitations

The response pattern examples used to test our hypothesis, and the CVR and type maps, are based on BOLD measurements, which were assumed to represent the *patterns* of cerebral blood flow responses to CO_2. BOLD provides a convenient surrogate of CBF, but the BOLD signal could be modulated by other factors (e.g., cerebral blood volume) in patients with advanced cerebrovascular disease. We do note that BOLD has been shown to be a reliable surrogate for CBF in patients [Mandell et al., 2008a] and so suggest that until shown to be different between patients and controls we accept BOLD as a reasonable surrogate for CBF. Both Duffin et al. [2015] and Tancredi et al. [2015] provide detailed discussions of the appropriateness of BOLD as a flow estimate and therefore are not repeated here. We therefore suggest that as a point of departure for the investigation of types of response patterns, and for the purposes of modelling, the patterns of BOLD response to a ramp PCO_2 stimulus are a reasonable representation of the flow patterns.

We point out that in this type of study the analysis is dependent on measuring arterial values of PCO_2. Therefore precise computer-controlled end tidal gas targeting, whether Dynamic End-tidal Forcing [Wise et al., 2007], or model-based prospective end-tidal gas targeting as with RespirAct™ is required. Applying methods that assume arterial PCO_2 values without having been validated against arterial blood gas samples will not be quantitative and may suffer from considerable errors that could significantly affect type classification. More primitive PCO_2 control schemes such as manually adding progressively higher concentrations of CO_2 to inspired gas lead to an inability to adequately control the actual stimulus, because the arterial PCO_2 is a function of the ventilatory response as well as the inspired CO_2 concentration [Fisher, 2016], and the ventilatory response varies between people and within people over time. An uncontrolled stimulus makes it very difficult to assess any aspect of CVR, and the lack of quality control makes it very difficult to compare or pool results between centres.

There are several factors that may affect the type classification. One that on first consideration might affect the type scoring is the dynamic properties of the response including the speed of response and transit time differences [Duffin et al., 2015; Poublanc et al., 2015]. However, we suggest that the slow rise of CO_2 during the ramp, and the maintenance of hypocapnia before the ramp, mitigates against any such an effect attaining significance. The type classification used only the ramp portion of the stimulus, which for both control and patient studies was sufficiently slow, even in the faster ramp of the patient study, that the responses could be considered steady state. Since the type classification was based solely on the sign of the linear slopes fitted to the hypo- and hypercapnic portions of the ramp response, the fact that the longer ramp measured in the control group contained more points, and would yield a possibly improved linear fit, therefore did not affect the type classification. We note also that possible errors in the choice of resting PCO_2 as the split point was not a critical factor in classification. For example the response shown in Figure 2 would be classified as a D −/+ type with the split chosen anywhere between 35 and 45 mm Hg.

Another factor is the overall responsiveness, with regions of low response potentially ambiguous as to type. Ancillary to the low responsiveness factor is that of noise in the BOLD signal. For example GM signal/noise is usually higher than that of WM, and control subject data less noisy than patient data, and so the signal/noise may affect the r^2 values for the linear slope fits. We note in particular that the prevalence of type D (−/+) is relatively higher in WM than GM in both patients and controls. It is therefore possible that the lower signal/noise values in WM compared with GM could have affected the type classification of WM voxels. We suggest

that such is not the case and that a pathophysiological explanation as yet unspecified underlies the development of type D (−/+) responses in WM. Our reasoning is as follows.

An advantage of the type classification is that it is based not on the slope values and quality of fit, which would be affected by the signal/noise ratio, but simply on the signs of the slopes of the linear fits. This aspect makes the type classification very robust, as all types are equally affected by signal/noise. Added to that is the accumulation of data points during the slow ramp increase of the stimulus, which ensures that many data points contribute to the fitting, and increasing the accuracy of the slope sign estimates. One observation that supports the robustness of type classification is the appearance of large confluent areas of the same type rather than a heterogeneous mixture of types in a brain region. However, there may be particular regions of the brain where caution in interpretation of CVR is required. For example, physiologically, we expect most of the frontal regions to behave as the rest of the brain, but we frequently see discordant responses in the anterior, inferior, medial portions of the frontal lobes. The unreliability of this signal is no different than fMRI studies that show similar deterioration of BOLD signal in this region well known to be secondary to magnetic susceptibility induced magnetic field distortions arising from the paranasal sinuses. Nevertheless, we have not seen significant CVR variability between lobes based on the database of normal controls that we have accumulated.

Finally, as an overriding caveat, it should be recognised that the interpretations of the type maps offered here are hypothesis generating speculations only, based on our current understanding of cerebral blood flow regulation, and require further experimental support.

CONCLUSIONS

Despite the traditional assumption of a linear or sigmoidal increase in cerebral blood flow in response to a progressive rise in $P_{ET}CO_2$, a comprehensive survey of voxels in healthy subjects and patients showed more complex response patterns. Classifying the response patterns into 4 distinct types to produce type maps enhances the interpretation of the linear regression CVR maps and, if pursued, will provide additional insight into cerebrovascular physiology and pathophysiology.

DISCLOSURE/CONFLICT OF INTEREST

JAF is Chief Scientist and JD is Senior Scientist at Thornhill Research Inc. (TRI), a spin-off company from the University Health Network that developed the RespirAct™. RespirAct™ is currently a non-commercial research tool assembled, and made available by TRI to research institutions to enable CVR studies.

REFERENCES

Battisti-Charbonney A, Fisher J, Duffin J (2011): The cerebrovascular response to carbon dioxide in humans. J Physiol 589: 3039–3048.

Bhogal A, Siero JC, Fisher JA, Froeling M, Luijten P, Philippens M, Hoogduin H (2014): Investigating the non-linearity of the BOLD cerebrovascular reactivity response to targeted hypo/hypercapnia at 7T. Neuroimage 98:296–305.

Bhogal AA, Philippens ME, Siero JC, Fisher JA, Petersen ET, Luijten PR, Hoogduin H (2015): Examining the regional and cerebral depth-dependent BOLD cerebrovascular reactivity response at 7T. Neuroimage 114:239–248.

Cox RW (1996): AFNI: Software for analysis and visualization of functional magnetic resonance neuroimages. Comput Biomed Res 29:162–173.

Duffin J, Sobczyk O, Crawley AP, Poublanc J, Mikulis DJ, Fisher JA (2015): The dynamics of cerebrovascular reactivity shown with transfer function analysis. Neuroimage 114:207–216.

Faraci F, Heistad D (1990): Regulation of large cerebral arteries and cerebral microvascular pressure. Circ Res 66:8–17.

Fierstra J, Winter J, Machina M, Lukovic J, Duffin J, Kassner A, Fisher J (2013): Non-invasive accurate measurement of arterial PCO2 in a pediatric animal model. J Clin Monit Comp 27:147–155.

Fisher JA (2016): The CO2 stimulus for cerebrovascular reactivity: Fixing inspired concentrations vs. targeting end-tidal partial pressures. J Cereb Blood Flow Metab 36:1004–1011.

Mandell DM, Han JS, Poublanc J, Crawley AP, Kassner A, Fisher JA, Mikulis DJ (2008a): Selective reduction of blood flow to white matter during hypercapnia corresponds with leukoaraiosis. Stroke 39:1993–1998.

Mandell DM, Han JS, Poublanc J, Crawley AP, Stainsby JA, Fisher JA, Mikulis DJ (2008b): Mapping cerebrovascular reactivity using blood oxygen level-dependent MRI in Patients with arterial steno-occlusive disease: Comparison with arterial spin labeling MRI. Stroke 39:2021–2028.

Pillai JJ, Mikulis DJ (2015): Cerebrovascular reactivity mapping: An evolving standard for clinical functional imaging. Am J Neuroradiol 36:7–13.

Poublanc J, Han JS, Mandell DM, Conklin J, Stainsby JA, Fisher JA, Mikulis DJ, Crawley AP (2013): Vascular steal explains early paradoxical blood oxygen level-dependent cerebrovascular response in brain regions with delayed arterial transit times. Cerebrovasc Dis Extra 3:55–64.

Poublanc J, Crawley AP, Sobczyk O, Montandon G, Sam K, Mandell DM, Dufort P, Venkatraghavan L, Duffin J, Mikulis DJ, Fisher JA (2015): Measuring cerebrovascular reactivity: The dynamic response to a step hypercapnic stimulus. J Cereb Blood Flow Metab 35:1746–1756.

Saad ZS, Glen DR, Chen G, Beauchamp MS, Desai R, Cox RW (2009): A new method for improving functional-to-structural MRI alignment using local Pearson correlation. Neuroimage 44:839–848.

Slessarev M, Han J, Mardimae A, Prisman E, Preiss D, Volgyesi G, Ansel C, Duffin J, Fisher JA (2007): Prospective targeting and control of end-tidal CO2 and O2 concentrations. J Physiol 581:1207–1219.

Sobczyk O, Battisti-Charbonney A, Fierstra J, Mandell DM, Poublanc J, Crawley AP, Mikulis DJ, Duffin J, Fisher JA (2014): A conceptual model for CO2-induced redistribution of cerebral blood flow with experimental confirmation using BOLD MRI. Neuroimage 92:56–68.

Sobczyk O, Battisti-Charbonney A, Poublanc J, Crawley AP, Sam K, Fierstra J, Mandell DM, Mikulis DJ, Duffin J, Fisher JA (2015):

Assessing cerebrovascular reactivity abnormality by comparison to a reference atlas. J Cereb Blood Flow Metab 35:213–220.

Somogyi RB, Vesely AE, Preiss D, Prisman E, Volgyesi G, Azami T, Iscoe S, Fisher JA, Sasano H (2005): Precise control of end-tidal carbon dioxide levels using sequential rebreathing circuits. Anaesth Intensive Care 33:726–732.

Tancredi FB, Lajoie I, Hoge RD (2015): Test-retest reliability of cerebral blood flow and blood oxygenation level-dependent responses to hypercapnia and hyperoxia using dual-echo pseudo-continuous arterial spin labeling and step changes in the fractional composition of inspired gases. J Magn Reson Imaging 42:1144–1157.

Wise RG, Pattinson KT, Bulte DP, Chiarelli PA, Mayhew SD, Balanos GM, O'Connor DF, Pragnell TR, Robbins PA, Tracey I, Jezzard P (2007): Dynamic forcing of end-tidal carbon dioxide and oxygen applied to functional magnetic resonance imaging. J Cereb Blood Flow Metab 27:1521–1532.